Journal of Pharmaceutical and Biomedical Analysis 55 (2011) 54–63

Contents lists available at ScienceDirect

Journal of Pharmaceutical and Biomedical Analysis

journal homepage: www.elsevier.com/locate/jpba

Unifying the mathematical modeling of *in vivo* and *in vitro* microdialysis

Peter M. Bungay[a,*], Rachita K. Sumbria[b], Ulrich Bickel[b]

[a] *Biomedical Engineering and Physical Science Shared Resource, National Institute of Biomedical Imaging and Bioengineering, National Institutes of Health, Building 13/3N17, Bethesda, MD 20892, USA*

[b] *Department of Pharmaceutical Sciences and Center for Vascular Drug Research, School of Pharmacy, Texas Tech University Health Science Centre, Amarillo, TX 79106, USA*

ARTICLE INFO

Article history:
Received 4 October 2010
Received in revised form 5 January 2011
Accepted 11 January 2011
Available online 19 January 2011

Keywords:
Microdialysis
Mathematical model
Extraction efficiency
Diffusion

ABSTRACT

A unifying approach is presented for developing mathematical models of microdialysis that are applicable to both *in vitro* and *in vivo* situations. Previous models for cylindrical probes have been limited by accommodating analyte diffusion through the surrounding medium in the radial direction only, i.e., perpendicular to the probe axis, or by incomplete incorporation of diffusion in the axial direction. Both radial and axial diffusion are included in the present work by employing two-dimensional finite element analysis. As in previous models, the nondimensional clearance modulus (Θ) represents the degree to which analyte clearance from the external medium influences diffusion through the medium for systems exhibiting analyte concentration linearity. Incorporating axial diffusion introduces a second dimensionless group, which is the length-to-radius aspect ratio of the membrane. These two parameter groups uniquely determine the external medium permeability, which is time dependent under transient conditions. At steady-state, the dependence of this permeability on the two groups can be approximated by an algebraic formula for much of the parameter ranges. Explicit steady-state expressions derived for the membrane and fluid permeabilities provide good approximations under transient conditions (quasi-steady-state assumption). The predictive ability of the unifying approach is illustrated for microdialysis of sucrose *in vivo* (brain) and inert media *in vitro*, under both well-stirred and quiescent conditions.

Published by Elsevier B.V.

1. Introduction

Application of microdialysis for *in vivo* sampling of drugs and diffusible constituents of tissue has benefited from the existence of mathematical models relating probe efficiencies to fundamental parameters characterizing probe geometry, analyte diffusion and tissue physiology. The models clarify the important interplay between analyte diffusion through and elimination from the tissue surrounding the microdialysis probe. To achieve simplicity in the descriptions, most of the existing models [1–9] assume cylindrical symmetry about the probe axis and restrict analyte diffusion to the radial direction perpendicular to the membrane. However, this restriction leads to a conundrum that the differential mass balance equations for the tissue do not admit useful steady-state solutions in the pure diffusion limit where there is no analyte elimination from the tissue. As a consequence, the purely radial diffusion models have limitations when applied to the analogous quasi-steady-state *in vitro* condition of a probe situated in an inert quiescent medium. Probes are typically immersed in an inert solution *in vitro* to assess their performance before or after *in vivo* use. The lack of models jointly applicable to common *in vitro* and *in vivo* situations is inherently unsatisfactory.

As a partial means of overcoming this limitation, an alternative model was proposed in which the probe is replaced by an equivalent sphere of the same area as the outer surface of the probe [3]. The primary appeal of this approach is that nontrivial solutions to the equations for diffusion in spherical geometry do exist. The applicability of this equivalent sphere model was postulated, but not convincingly demonstrated. Uncertainty about the quantitative validity of this approximation has limited its usefulness.

Instead of employing models posed in different geometries, a more rational scheme is to construct models in two- or three-dimensional geometries that would be applicable to a wide range of operating conditions. In recognizing the desirability of this goal, Tong and Yuan [10] formulated a two-dimensional model for *in vivo* sampling that includes both axial and radial diffusion within the tissue. Their analysis involved simultaneously simulating analyte transport through tissue, membrane and perfusate fluid. The authors elegantly proposed replacing the nominal membrane length by a larger equivalent length to represent the two-dimensional effects of diffusion and elimination within the tissue. This concept has the advantage of retaining in slightly modified form the closed-form expressions from the previous linear steady-state model for radial diffusion. However, this empirical

* Corresponding author. Tel.: +1 301 435 1942; fax: +1 301 496 6608.
E-mail address: bungayp@mail.nih.gov (P.M. Bungay).

0731-7085/$ – see front matter. Published by Elsevier B.V.
doi:10.1016/j.jpba.2011.01.005

Nomenclature

c	analyte concentration
C	normalized two-dimensional analyte concentration profile
D	diffusion coefficient
E	extraction fraction
h	Amberg and Lindefors function, Eq. (22)
J	Bessel functions of the first kind
k	clearance rate constant
K	modified Bessel functions of the second kind
K	equilibrium distribution coefficient
L	length
P	diffusive permeability
$\hat{P}$	overall diffusive permeability for the probe and external medium
q	analyte mass flow rate
Q	volumetric flow rate
r	radial position relative to probe axis
S	superficial area of membrane exchange surface
t	time
T	time constant
u	dummy variable of integration
U	normalized one-dimensional radial concentration profile
v	velocity
Y	Bessel functions of the second kind
z	axial position relative to inlet end of membrane exchange surface

Greek letters

ϕ	extracellular volume
γ	dimensionless ratio of annulus radii, Eq. (9)
Γ	penetration depth, Eq. (24)
λ	empirical constant in the equivalent membrane length model, Eq. (36)
ϖ	radial position for equivalent spherical probe model
Θ	clearance modulus, Eq. (21)
ρ	dimensionless radial position, Eq. (15)
τ	dimensionless time, Eq. (15)
ζ	dimensionless axial position, Eq. (15)

Subscripts

a	annulus
$cann$	inner cannula
e	external medium, free
ext	external medium, total
E	equivalent
i	inner surface of membrane
in	inlet end of membrane exchange surface
m	membrane; based on whole membrane volume
o	outer surface of membrane
out	outlet end of membrane exchange surface or outflow tubing
$\wp$	probe (annulus fluid + membrane)
s	equivalent spherical probe
ws	well-stirred conditions
∞	spatial asymptote in radial or axial direction

Superscripts

1D	one-dimensional (radial diffusion)
2D	two-dimensional (radial and axial diffusion)
Sph	equivalent spherical probe

Diacritical marks

$\bar{}$	flow-rate-weighted radial average in the annulus

Brackets

[ ]	follows a function symbol to indicate the variables upon which it depends

modification does not exhibit the appropriate character in the pure diffusion limit and consequently is not generally applicable to *in vitro* measurements.

The present approach similarly involves two-dimensional modeling for radial and axial diffusion through the medium external to the probe. The approach employs approximations that permit the results to be encompassed within the framework of earlier linear models [3,7–10]. The outcome is an illustrative unified model of transient and steady-state microdialysis applicable for both *in vivo* and *in vitro* conditions.

2. Linear microdialysis theory

Microdialysis employs a perfused probe with a solute permeable membrane that permits exchange between the perfusate solution and the external medium into which the probe has been implanted. Differences in free solute concentration between the external medium and the perfusate promote exchange by diffusion. The membrane is likely to be permeable as well to fluid so that solute may be carried across the membrane convectively, if significant transmembrane fluid flow takes place. Although transmembrane convection can be incorporated [11,12], the model to be presented is based on the customary assumption that diffusion is the dominant mechanism within the membrane. A number of additional assumptions are invoked in common with earlier versions [3,5,9]. Principally, these are simplifications to render the governing equations linear with respect to analyte concentration, such as assuming that analyte clearance processes depend linearly on analyte concentration and physical properties are independent of concentration. The presentation begins with an overview of the previous modeling approach that restricted diffusion within the external medium to the radial direction. This provides the context for the subsequent generalization that adds the effects of axial diffusion.

2.1. Steady-state radial diffusion model

Diffusion of analyte across the membrane is driven by the difference in free concentrations, c_i and c_o at the inner and outer surfaces, respectively. Let the membrane permeability, P_{m_o}, be the coefficient of proportionality between the concentration difference and the analyte mass flow rate, q. For steady-state conditions at any axial position, z, the outward differential mass flow rate is represented by

$$dq[z] = 2\pi r_o \cdot P_{m_o} \cdot (c_i[z] - c_o[z]) \cdot dz. \quad (1)$$

The subscript, "o", indicates that the permeability is referenced to the outer surface area of the membrane of outer radius, r_o. The analyte flux into the membrane is supplied by the perfusate flowing in the annular space between the membrane and the internal cannula. An alternate expression for the differential rate is then

$$dq[z] = 2\pi r_o \cdot P_{a_o} \cdot (\bar{c}_a[z] - c_i[z]) \cdot dz, \quad (2)$$

where $\bar{c}_a$ is the flow weighted annulus bulk concentration and P_{a_o} is the permeability in the annular fluid. Similarly, for the mass flow

from the membrane into the external medium,

$$dq[z] = 2\pi r_o \cdot P_{ext_o} \cdot (c_o[z] - c_{e_\infty}) \cdot dz. \tag{3}$$

In the above, it is assumed that the free concentration in the external medium far from the probe is spatially uniform, as indicated by c_{e_∞}, and also that all three permeabilities are uniform, i.e., independent of z. Combining Eqs. (1)–(3) leads to

$$dq[z] = 2\pi r_o \cdot \hat{P}_o \cdot (\bar{c}_a[z] - c_{e_\infty}) \cdot dz, \tag{4}$$

in which $\hat{P}_o$ is an overall permeability,

$$\hat{P}_o \equiv \left(\frac{1}{P_{a_o}} + \frac{1}{P_{m_o}} + \frac{1}{P_{ext_o}} \right)^{-1}. \tag{5}$$

Equating the mass flow rate, q, to the rate of analyte loss from the perfusate gives,

$$-\ Q_a \frac{d\bar{c}_a}{dz} = 2\pi r_o \cdot \hat{P}_o \cdot (\bar{c}_a - c_{e_\infty}), \tag{6}$$

with Q_a denoting the volumetric flow rate of the annulus fluid. Integrating over the length, L_m, of the portion of membrane accessible for analyte permeation yields the following exponential expression for the efficiency of extracting the analyte from the perfusate,

$$E \equiv \frac{c_{in} - c_{out}}{c_{in} - c_{e_\infty}} = 1 - \exp\left[-\frac{\hat{P}_o \cdot S_o}{Q_a} \right], \tag{7}$$

in which $c_{in} = \bar{c}_a[0]$ and $c_{out} = \bar{c}_a[L_m]$ are the perfusate inflow and dialysate outflow concentrations, respectively, and $S_o = 2\pi \cdot r_o \cdot L_m$ is the accessible area of the outer surface of the membrane. For analyte diffusion and elimination rates in the external medium that are linear in analyte concentration, Eq. (7) is independent of the direction of diffusion. In other words, the extraction efficiency should be the same for sampling analyte from the external medium as for delivering analyte from the perfusate to the external medium.

Except in the absence of an internal cannula, the magnitude of the annulus permeability, P_{a_o}, in Eq. (2) can be estimated from the following modified form of an asymptotic expression obtained by Bungay et al. [12],

$$P_{a_o} \approx \left(\frac{2.0 + 0.42 \cdot \gamma}{1 - \gamma} \right) \cdot \left(\frac{D_a}{r_o} \right), \tag{8}$$

in which D_a is the analyte free solution diffusion coefficient and γ is the annulus radius ratio,

$$\gamma \equiv \frac{r_{cann}}{r_i}, \tag{9}$$

involving the outer radius of the cannula, r_{cann}. For probes lacking an internal cannula the approximate expression reduces to $P_{a_o} \approx 1.83 D_a / r_o$. The membrane permeability is given by,

$$P_{m_o} = \frac{D_m}{r_o \ln[r_o / r_i]}, \tag{10}$$

with D_m being the effective diffusion coefficient for the analyte [9].

2.2. Transient radial diffusion model

As shown by Morrison et al. [4] and Chen et al. [7,8], restricting diffusion to the radial direction renders the governing equations amenable to analytical solutions for transient behavior as well. In their approach Morrison et al. [4] invoked a quasi-static approximation for the probe. Analyte transport in the annulus and membrane was assumed to adjust much more rapidly to change than the external medium because of the large differences in capacity for the analyte. By neglecting the contribution of diffusion to transport in the annulus, Chen et al. [7,8] were able to express transient behavior in both the membrane and the external medium. The present treatment is equivalent to that of Morrison et al. [4] in employing steady-state expressions for the annulus and membrane permeabilities, Eqs. (8) and (10), but expresses the transient behavior for the external medium in terms of the permeability. As in the previous models, the external medium is assumed to consist of two phases with spatial uniform properties. For *in vivo* applications the two phases are the extracellular space and the cellular phase. In the extracellular space the variation in the free concentration of the diffusible analyte of interest over space and time, t, will be denoted by $c_e[r, z, t]$. The ratio of the total concentration of the analyte, $c_{ext}[r, z, t]$, to the free concentration will be represented by

$$K_{ext} \equiv \frac{c_{ext}}{c_e}. \tag{11}$$

This distribution coefficient is taken to be a constant by the assumption of local equilibrium for any binding and exchange between extracellular and intracellular compartments [9].

For the radial diffusion model the local variations in the concentrations are determined by a differential mass balance for the analyte of the form

$$K_{ext} \frac{\partial c_e}{\partial t} = D_{ext} \frac{1}{r} \frac{\partial}{\partial r} \left(r \frac{\partial c_e}{\partial r} \right) - k_{ext} \cdot c_e, \tag{12}$$

in which D_{ext} is the diffusion coefficient for the analyte in the external medium. The rates of processes that eliminate analyte from the external medium are assumed to be proportional to the local free concentration, so that k_{ext} is an overall first order rate constant for these linear clearance mechanisms. The basis for both D_{ext} and k_{ext} is the total volume of the external medium volume, i.e., the sum of the excellular and cellular volumes [9].

Far from the probe the free extracelluar concentration approaches a uniform value

$$c_e[r, z, t] \to c_{e_\infty} \quad \text{as} \quad r \to \infty. \tag{13}$$

As in Morrison et al. [4], the distant concentration could vary with time. For the objectives of this presentation, c_{e_∞} will be considered a constant. The initial condition takes the distant concentration to be the uniform value throughout the external medium

$$c_e[r, z, 0] = c_{e_\infty} \quad \text{at} \quad t = 0. \tag{14}$$

It is advantageous to redefine the independent variables in dimensionless form

$$\rho \equiv \frac{r}{r_o}, \quad \zeta \equiv \frac{z}{r_o} \quad \text{and} \quad \tau \equiv \frac{t}{T_{ext}}. \tag{15}$$

Time is scaled in Eq. (15) relative to the time constant for diffusion in the external medium,

$$T_{ext} \equiv \frac{r_o^2 \cdot K_{ext}}{D_{ext}}. \tag{16}$$

As noted by Chen et al. [7,8], the separation of variables solution to Eqs. (12)–(16) can be expressed in terms of a normalized one-dimensional (1D) radial concentration profile that is independent of axial position

$$U[\rho, \tau] \equiv \frac{c_e[\rho, \zeta, \tau] - c_{e_\infty}}{c_e[1, \zeta, \tau] - c_{e_\infty}}. \tag{17}$$

The value of the profile, U, at the membrane interface is

$$U[1, \tau] = 1. \tag{18}$$

The external medium permeability is related to the diffusive flux across the membrane interface. In terms of the normalized 1D profile the relationship can be expressed as

$$P_{ext_o}^{1D}[\tau] = -\frac{D_{ext}}{r_o} \left(\frac{\partial U[\rho, \tau]}{\partial \rho} \right)_{\rho=1}. \tag{19}$$

The following expression for the normalized transient permeability is readily obtained from the solution for $U[\rho, \tau]$ derived by Chen et al. [8]

$$\frac{r_o \cdot P^{1D}_{ext_o}[\tau]}{D_{ext}} = \frac{\Theta \cdot K_1[\Theta]}{K_0[\Theta]} + \frac{4}{\pi^2}\int_0^\infty \frac{u \cdot \exp[-(u^2+\Theta^2)\cdot\tau]}{(u^2+\Theta^2)\cdot(J_0^2[u]+Y_0^2[u])}\,du, \tag{20}$$

in which K_0 and K_1 are the modified Bessel functions of the second kind of order zero and one, J_0 and Y_0 are the Bessel functions of the first and second kind of order zero and u is a dummy variable of integration. The Bessel functions appear in Eq. (20) as a consequence of the cylindrical geometry. These standard mathematical functions are available in spreadsheet software and handbooks, such as Abramowitz and Stegun [13]. The argument, Θ, is a dimensionless clearance modulus defined as

$$\Theta \equiv r_o\sqrt{\frac{k_{ext}}{D_{ext}}}. \tag{21}$$

Eq. (20) is valid for all Θ and simplifies in the zero clearance limit to the following form involving the integral function, $h[\tau]$, defined by Amberg and Lindefors [1]

$$\frac{r_o}{D_{ext}}(P^{1D}_{ext_o}[\tau])_{\Theta=0} = 2\cdot h[\tau] \equiv \frac{4}{\pi^2}\int_0^\infty \frac{\exp[-u^2\cdot\tau]}{J_0^2[u]+Y_0^2[u]}\frac{du}{u}. \tag{22}$$

The value of the integral on the right-hand-side of Eq. (20) decays to zero as $\tau \to \infty$ reducing the overall expression to the steady-state result obtainable from the mass transfer resistance of Bungay et al. [3]

$$\frac{r_o \cdot P^{1D}_{ext_o}}{D_{ext}} = \frac{\Theta \cdot K_1[\Theta]}{K_0[\Theta]}. \tag{23}$$

The square root term in Eq. (21) constitutes a characteristic length scale,

$$\Gamma \equiv \sqrt{\frac{D_{ext}}{k_{ext}}}. \tag{24}$$

This quantity has been referred to as the penetration depth [3], since it provides a measure of the distance within the external medium over which analyte concentration is perturbed by the diffusional exchange with the probe at steady state. However, in the absence of analyte clearance, $\Gamma \to \infty$ since $k_{ext} = 0$. An infinite penetration depth is a physically unrealistic interpretation for Γ. This impractical limit is avoided by incorporating axial diffusion, as in the following section.

The radial diffusion model does have a useful limit for $P^{1D}_{ext_o} \to \infty$ corresponding to the probe immersed in a well-stirred fluid medium. For this condition the overall permeability in Eq. (5) reduces to the probe permeability

$$P_{\wp_o} \equiv \left(\frac{1}{P_{a_o}} + \frac{1}{P_{m_o}}\right)^{-1}. \tag{25}$$

The probe permeability can then be determined from a measurement of the extraction fraction under the well-stirred condition, E_{ws},

$$P_{\wp_o} = -\left(\frac{Q_a}{S_o}\right)\cdot\ln[1-E_{ws}]. \tag{26}$$

Diffusion in the axial direction is expected to be a minor contributor to the annulus and membrane permeability. By contrast, axial diffusion can have a pronounced influence on the external medium permeability, as demonstrated below.

2.3. Radial and axial diffusion in isolated external medium

As a consequence of ignoring axial diffusion, the membrane length does not appear in the 1D permeability expressions (8), (10) and (20)–(23). The only explicit influence of membrane length on extraction efficiency arises from the membrane area term, S_o, in Eq. (7). This section describes a two-dimensional (2D) approach to including axial diffusion that introduces dependence on membrane length missing from the 1D radial diffusion model. The approach uses the geometry shown in Fig. 1(a) and considers the external medium in isolation from the probe. By analogy with the 1D normalized concentration, U, in definition (17), this approach seeks a normalized 2D concentration profile defined as

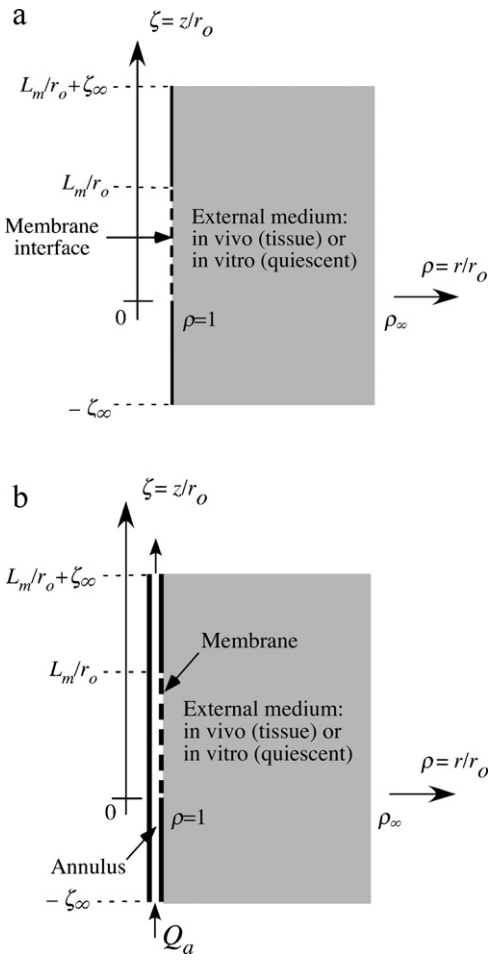

Fig. 1. Schematics for two-dimensional (2D) models in which diffusion occurs in both radial and axial directions. (a) Isolated external medium with a source of uniform dimensionless concentration, $C = 1$, along the membrane interface and $C = 0$ on the distant dimensionless boundaries at $\rho_\infty = r_\infty/r_o$ and $\zeta = \pm z_\infty/r_o$. (b) Combined probe (annular fluid and membrane) and external medium. The annular fluid is in steady, laminar flow at the volumetric rate, Q_a, with inlet concentration, $\bar{C}_a = 1$. On the distant external medium boundaries, $C = 0$. To aid in visualization, the radial scale of the perfusate and membrane regions have been expanded relative to the distant boundaries. The radial and axial positions and membrane length, L_m, have been nondimensionalized with respect to membrane outer radius, r_o.

$$C[\rho, \zeta, \tau] \equiv \frac{c_e[\rho, \zeta, \tau] - c_{e_\infty}}{c_e[1, \zeta, \tau] - c_{e_\infty}}, \tag{27}$$

subject to the boundary conditions at the membrane interface

$$C[\rho, \zeta, \tau] = 1 \quad \text{at} \quad \rho = 1, \tag{28}$$

and far from the membrane where the concentration approaches the constant, uniform value

$$C[\rho, \zeta, \tau] \to 0 \quad \text{for large} \quad \rho_\infty \quad \text{or} \quad \zeta_\infty, \tag{29}$$

as well as the corresponding initial condition of uniform concentration throughout the external medium

$$C[\rho, \zeta, 0] = 0 \quad \text{at} \quad \tau = 0. \tag{30}$$

The nondimensional differential mass balance takes the form

$$\frac{\partial C}{\partial \tau} = \frac{1}{\rho}\frac{\partial}{\partial \rho}\left(\rho \frac{\partial C}{\partial \rho}\right) + \frac{\partial^2 C}{\partial \zeta^2} - \Theta^2 \cdot C. \tag{31}$$

Eq. (31) was integrated numerically throughout the external medium subject to the boundary and initial conditions (28)–(30). Solutions were obtained using the finite element software, Comsol Multiphysics (Comsol, Inc., Burlington, MA). Values for $P_{ext_o}^{2D}$ were obtained in normalized form from the definition

$$\frac{r_o \cdot P_{ext_o}^{2D}[\tau]}{D_{ext}} \equiv -\frac{r_o}{L_m}\int_0^{L_m/r_o}\left(\frac{\partial C[\rho, \zeta, \tau]}{\partial \rho}\right)_{\rho=1} d\zeta. \tag{32}$$

Eqs. (28)–(32) reveal that the normalized permeability is a function of time and only the two dimensionless parameters, Θ and L_m/r_o, provided that the values of ρ_∞ and ζ_∞ are chosen to be sufficiently large. The above numerical approach yields equivalent predictions to those of the radial model, if the external medium geometry in Fig. 1(a) is collapsed by setting $\zeta_\infty = 0$. For example, simulations for the permeability would then be in agreement with Eqs. (20), (22) and (23) for all values of Θ.

2.4. Full model for validation of the isolated external medium permeability model

The utility of the isolated external medium model was investigated by comparing predictions with those from a full finite element model combining the probe with the external medium. The geometry for this more detailed model is shown schematically in Fig. 1(b). The Navier–Stokes equations were solved to obtain the perfusate velocity profile in the annular space between an inner cannula of radius, r_{cann}, and the membrane inner surface of radius, r_o. Then the differential mass balance equation for analyte convection and diffusion was solved for the annulus. Simultaneously, the mass balance corresponding to Eq. (31) was solved for the external medium, together with a similar equation for the membrane but without the elimination term. Instead of Eq. (27), the normalized 2D concentration was redefined as

$$C[\rho, \zeta, \tau] = \frac{c[\rho, \zeta, \tau] - c_{e_\infty}}{c_{in} - c_{e_\infty}}, \tag{33}$$

so that at the inlet, $\bar{C}_a[0, \tau] = 1$, and at the distant boundaries, $C = 0$. Comsol Multiphysics was used for all of the simulations. To provide specific examples for applying the unified model to both *in vitro* and *in vivo* conditions, microdialysis of sucrose was simulated for a probe implanted in a gel (representing an inert, quiescent medium) and in mouse brain. The parameter values required for the simulations are presented in Tables 1–4. Table 1 contains the geometric parameters values for a custom-made probe with a cellulosic membrane. Table 2 provides the permeabilities and diffusion coefficient values estimated for sucrose in the annulus and membrane utilizing measurements *in vitro* in a well-stirred solution. Tables 3 and 4 list the parameter values for sucrose microdialysis in the gel and in mouse brain, respectively.

3. Experiments

3.1. Probe calibration in a well-stirred solution

Dialysis probes were immersed in a 20-mL beaker containing 0.5 μCi of ^{14}C-sucrose dissolved in an artificial cerebrospinal fluid (aCSF) that was well-stirred and maintained at 37 °C. The concentration of ^{14}C in this external medium, c_{e_∞}, was determined from triplicate 100-μL aliquots. The probe was perfused with aCSF at a volumetric flow rate of 2 μL/min and dialysate samples were collected in pre-weighed vials at intervals of 10 min for 60 min for measurement of the outflow concentration, c_{out}. Each sample was diluted with 5 mL of liquid scintillation cocktail (ScintiSafe 30%, Fisher Scientific, Fair Lawn, NJ) and counted for 10 min using a liquid scintillation counter (LS6000SC, Beckman Instruments Inc., Fullerton, CA) with an efficiency of 95% for ^{14}C activity. Extraction fraction was calculated from Eq. (7) reduced to the form for sampling

$$E_{ws} = \frac{c_{out}}{c_{e_\infty}}. \tag{34}$$

The probe permeability, $P_{\wp_o}$, was calculated from E_{ws} using Eq. (26) and this value was then used to obtain the membrane permeability, P_{m_o}, from Eq. (25) after estimating the annulus permeability, P_{a_o}, from Eq. (8). The membrane permeability was used to calculate the effective membrane diffusion coefficient from Eq. (10). The calculations employed the geometric parameter values from Table 1.

3.2. Transient extraction fraction measurement for probes inserted into gel

A 0.3% (w/v) solution of agarose in aCSF was prepared by adding agarose to warm aCSF in a 100-mL beaker (6-cm dia; 6-cm height). After the addition of 15 μCi of ^{14}C-sucrose, triplet 10-μL aliquot samples were taken for the determination of the activity, c_{e_∞}. The solution was then gelled by cooling and a microdialysis probe was implanted into the gel under stereotaxic control. The assembly, including the perfusate syringe and pump, was placed in an incubator and allowed to equilibrate to the set temperature of 37 °C. The probe was perfused at 2 μL/min and dialysate samples were collected in pre-weighed vials at intervals of 10 min for 120 min. Each sample was diluted with 5 mL of liquid scintillation cocktail (ScintiSafe 30%, Fisher Scientific, Fair Lawn, NJ) and counted for 10 min using a liquid scintillation counter (LS6000SC, Beckman Instruments Inc., Fullerton, CA) with an efficiency of 95% for ^{14}C activity. The outflow activity, c_{out}, was divided by c_{e_∞} as in Eq. (34) to obtain the variation over time in the sampling extraction fraction, E_{gel}.

4. Results and discussion

4.1. External medium permeability for diffusion restricted to the radial direction

When diffusion is restricted to the radial direction, the normalized external medium permeability is a function only of time (when expressed nondimensionally) and the clearance modulus, Θ. This 1D permeability is applicable only to probes of long membrane aspect ratio ($L_m/r_o \to \infty$). The time variation is illustrated in Fig. 2(a) for arbitrary values of the modulus over the partial range, $0 \le \Theta \le 1$. The smaller the modulus value, the slower the approach to steady-state and the lower the steady-state permeability. For zero clearance ($\Theta = 0$), the approach to steady-state is extremely slow and the steady-state 1D permeability value is zero. The dotted lines indicate the result for the arbitrary dimensionless time of $\tau = 100$ chosen by Chen et al. [8] to represent a quasi-steady-state for microdialysis in a gel. The normalized 1D permeability value at this arbitrary time point, $\tau = 100$, is 0.36.

Table 1
Geometric parameters values for custom probes constructed with cellulosic membrane.

Symbol	Description	Value	Units	Source
L_m	Length of accessible membrane	0.2	cm	Nominal value
r_{cann}	Outer radius of probe internal cannula	0.0075	cm	Measured
r_i	Membrane inner radius	0.0120	cm	Nominal value
r_o	Membrane outer radius	0.0140	cm	Nominal value
γ	Annulus radius ratio	0.61	–	r_{cann}/r_i
L_m/r_o	Membrane aspect ratio	14.3	–	

Table 2
Model parameters values for microdialysis of sucrose *in vitro* for probes from Table 1 immersed in a well-stirred solution at 37 °C.

Symbol	Description	Value	Units	Source
Q_a	Perfusate volumetric flow rate	2	μL/min	Calibrated pump setting
E_{ws}	Concentration extraction fraction	0.12 ± 0.01	–	Measured (mean ± SD, $n = 4$)
$P_{\wp_o}$	Probe diffusive permeability	0.014	cm/min	$-(Q_a/S_o) \cdot \ln[1 - E_{ws}]$, Eq. (26)
D_a	Free solution diffusion coefficient	4.2×10^{-4}	cm^2/min	Aqueous solution at 37 °C [15]
P_{a_o}	Steady-state annulus diffusive permeability	0.18	cm/min	$\left(\frac{2.0+0.42*\gamma}{1-\gamma}\right) \cdot \left(\frac{D_a}{r_o}\right)$, Eq. (8)
P_{m_o}	Steady-state membrane diffusive permeability	0.015	cm/min	$\left(\frac{1}{P_{\wp_o}} - \frac{1}{P_{a_o}}\right)^{-1}$, Eq. (25)
D_m	Effective diffusion coefficient in membrane	3.2×10^{-5}	cm^2/min	$P_{m_o} \cdot r_o \cdot \ln[r_o/r_i]$, Eq. (10)

Table 3
Model parameters values for microdialysis of sucrose *in vitro* for probes from Table 1 implanted in an inert, quiescent aqueous medium (0.3% agarose gel) at 37 °C.

Symbol	Description	Value	Units	Source
Q_a	Perfusate volumetric flow rate	2	μL/min	Calibrated pump setting
$D_{ext} = D_a$	Diffusion coefficient	4.2×10^{-4}	cm^2/min	Aqueous solution at 37 °C [15]
k_{ext}	Clearance rate constant	0	–	Inert medium
K_{ext}	Distribution coefficient	1	–	Nominal value
T_{ext}	Diffusion time constant	0.47	min	$r_o^2 \cdot K_{ext}/D_{ext} = r_o^2/D_a$
Θ	Clearance modulus	0	–	$r_o\sqrt{k_{ext}/D_{ext}}$, Eq. (21)
$P^{2D}_{ext_o}[t \to \infty]$	Steady-state 2D permeability	0.012	cm/min	Simulation

4.2. External medium permeability generalized by including the effects of axial diffusion

Under most microdialysis conditions, the direction of analyte diffusion in the adjacent medium is only constrained by the presence of impermeable obstacles, such as the probe shaft, and the diffusional properties of the medium. Incorporating diffusion in both radial and axial directions in the model simulations produces changes in both the magnitude and time course of the medium permeability. As illustrated in Fig. 2(b), for most of the Θ range the transients in the 2D permeability are similar in shape to corresponding 1D results displayed in Fig. 2(a). Including axial diffusion leads to significant increases in the 2D permeability values relative to the 1D radial diffusion predictions even for the relatively high aspect ratio of $L_m/r_o = 33.3$ used in these example calculations. The difference is progressively greater for small values of Θ. The effect is most noticeable for zero clearance ($\Theta = 0$), where decay is still slow at long times, but the 2D permeability does approach a finite value as $t \to \infty$. Thus, including axial diffusion obviates the need expressed by Chen et al. [8] to postulate that the transient achieves a quasi-steady state at the arbitrary dimensionless time of 100. The asymptotic value from the 2D simulation in Fig. 2(b) is 0.32, which is close to the value of 0.36 for the assumed quasi-steady state 1D result shown in Fig. 2(a).

The dependence of the normalized external medium 2D permeability on the second dimensionless parameter, L_m/r_o, is illustrated for steady-state conditions in Fig. 3. The abscissa in Fig. 3 is the clearance modulus defined in Eq. (21). The permissible range for the modulus is $0 \le \Theta < \infty$, but only results for the range $0 \le \Theta \le 1$ are shown. The family of solid curves results from selecting arbitrary values for the aspect ratio. As an example, the curve labeled $L_m/r_o = 4$ corresponds to commercially available probes with a membrane diameter of 0.5 mm and a length of 1 mm. The prediction from the 1D radial diffusion model, Eq. (23), is included as the lower-most curve corresponding to $L_m/r_o \to \infty$.

The solid curves in Fig. 3 are nearly straight lines except at low values of Θ and large values of L_m/r_o. The nearly straight portions

Table 4
Model parameters values for microdialysis of sucrose *in vivo* for probes from Table 1 implanted in mouse brain.

Symbol	Description	Value	Units	Source
Q_a	Perfusate volumetric flow rate	2	μL/min	Calibrated pump setting
D_e	Extracellular diffusion coefficient	1.86×10^{-4}	cm^2/min	Dog caudate [15]
ϕ_e	Extracellular volume fraction	0.2	–	Nominal value
D_{ext}	Diffusion coefficient in tissue	3.7×10^{-5}	cm^2/min	$D_e \cdot \phi_e$
k_{ext}	Rate constant for elimination from tissue	1.9×10^{-3}	mL/(min cm^3)	Unpublished measurements
K_{ext}	Distribution coefficient	0.2	–	ϕ_e
T_{ext}	Diffusion time constant in tissue	1.05	min	$r_o^2 \cdot K_{ext}/D_{ext} = r_o^2/D_e$
Θ	Clearance modulus	0.1	–	$r_o\sqrt{k_{ext}/D_{ext}}$, Eq. (21)
$P^{2D}_{ext_o}[t \to \infty]$	Steady-state tissue 2D permeability	0.0013	cm/min	Simulation

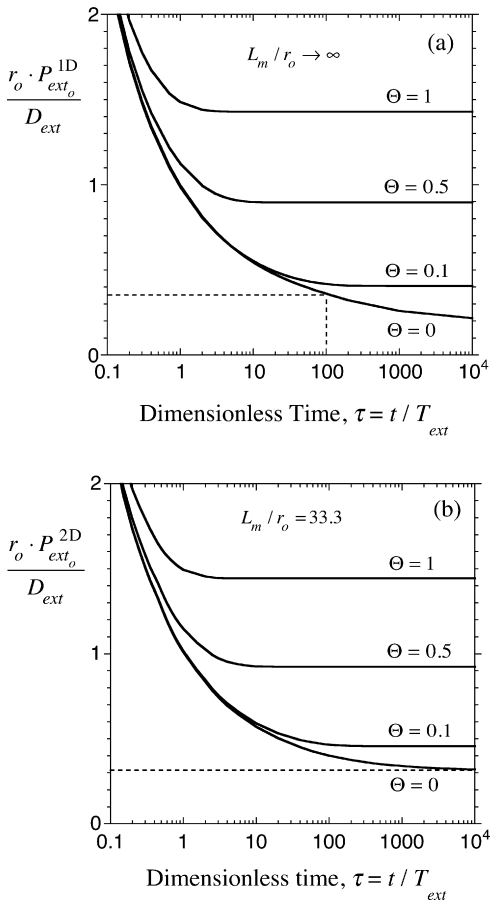

Fig. 2. Transients in the external medium permeability normalized with respect to the membrane outer radius, r_o, and the analyte diffusion coefficient, D_{ext}. Time, t, is nondimensionalized relative to the diffusion time constant, $T_{ext} = r_o^2/D_{ext}$. The arbitrary values of the clearance modulus represent only a portion of the range, $0 \le \Theta = r_o\sqrt{k_{ext}/D_{ext}} < \infty$, where k_{ext} is an overall first order rate constant for the processes removing analyte from the medium. (a) One-dimensional model (1D) in which diffusion is restricted to the radial direction. Applicable only to microdialysis probes for which the ratio of membrane length, L_m, to outer radius is high ($L_m/r_o \to \infty$). (b) Two-dimensional model (2D) that includes both axial and radial diffusion for an illustrative aspect ratio of 33.3 corresponding to the probes used by Höistad et al. [16].

can be well represented by the following algebraic formula

$$\frac{r_o \cdot P^{2D}_{ext_o}}{D_{ext}} = 0.4 + 1.01 \cdot \Theta + \frac{1.2 r_o}{L_m}. \quad (35)$$

Eq. (35) yields approximate permeability values for current commercially available probes, whose aspect ratios range within about $4 < L_m/r_o < 100$.

The intercepts on the vertical axis ($\Theta = 0$) in Fig. 3 represent the behavior expected for a probe in an inert quiescent medium, such as a gel. For the radial diffusion model the inert quiescent medium steady-state is represented by the origin where the permeability is zero, as no additional solute enters or leaves the external medium. This would correspond to a uniform dimensionless concentration of $U = 1$, which is in conflict with the distant boundary condition requiring $U \to 0$ as $\rho \to \infty$. By contrast, including axial diffusion in a large, but finite, external medium creates the possibility for steady-state solutions that are insensitive to the size of the medium. These steady-state solutions for probes with finite aspect ratios yield the nonzero 2D permeability values given by the intercepts on the vertical axis in Fig. 3.

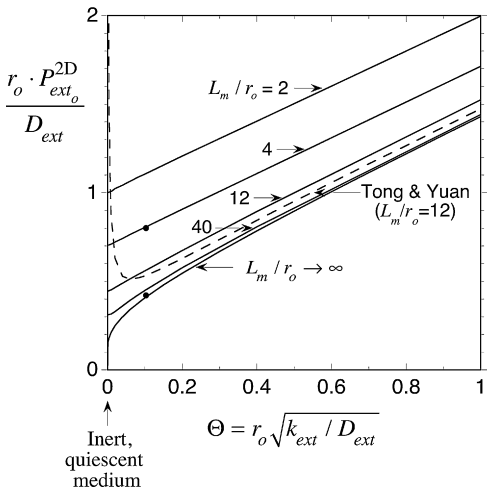

Fig. 3. Steady-state values for external medium permeabilities from the isolated medium 2D model with radial and axial diffusion. Axial diffusion results in an increase in the external medium permeability. The magnitude of the effect is a function of the membrane length-to-outer radius aspect ratio, L_m/r_o, and the analyte clearance modulus, Θ. The latter is the dimensionless ratio of the first order clearance rate constant, k_{ext}, and the effective diffusion coefficient, D_{ext}, defined in Eq. (21). Solid curves are predictions for arbitrary choices of the aspect ratio, except for the lower-most curve (labeled $L_m/r_o \to \infty$) from Eq. (23) for 1D diffusion restricted to the radial direction. The intercepts on the vertical axis represent behavior for an inert ($\Theta = 0$), quiescent medium. The dashed lines are the prediction from the equivalent length model of Tong and Yuan [10], Eq. (37). The filled circles denote the illustrative steady-state limits for $\Theta = 0.1$ from the transient predictions in Fig. 4.

The incorporation of axial diffusion led Tong and Yuan [10] to propose the concept of an equivalent length defined as

$$L_E = L_m + \lambda \cdot \Gamma, \quad (36)$$

in which λ is an empirical constant with an estimated value of 0.369 and Γ is the penetration depth from Eq. (24). Recasting the Tong and Yuan result in terms of the external medium permeability yields

$$\frac{r_o \cdot P^{2D}_{ext_o}}{D_{ext}} = \frac{\Theta + \lambda(r_o/L_m)}{K_0/K_1}. \quad (37)$$

Eq. (37) is plotted as the dashed curve in Fig. 3 for the aspect ratio that Tong and Yuan used in their simulations, $L_m/r_o = 12$. Their curve parallels the 2D isolated medium model results for most of the Θ range. However, the equivalent length model fails for values of Θ approaching zero and is thus not applicable to conditions in which there are no analyte clearance processes, such as an inert quiescent medium.

Axial diffusion affects the nature of transient, as well as steady-state, microdialysis. Nondimensionalizing the governing equations generalizes the predictions. *In vivo* microdialysis inherently involves an initial transient as illustrated in Fig. 4 for simulations of sucrose microdialysis in mouse brain characterized by the clearance modulus value of $\Theta = 0.1$ from Table 4. The two curves bracket the range of aspect ratios for the available commercial probes. Shorter probes yield faster transients, as well as higher permeabilities. The permeability decays to within 10% of the steady-state value by 6 min ($\tau = 12$) for $L_m/r_o = 4$, as contrasted with 16 min ($\tau = 35$) for $L_m/r_o = 100$ for the same criterion. The steady-state values from Fig. 4 correspond to the two filled circles in Fig. 3.

4.3. Extraction efficiency

To demonstrate the unified applicability, the proposed modeling approach was applied to determining the transient and steady-state extraction fractions for sucrose under both *in vitro* and *in vivo*

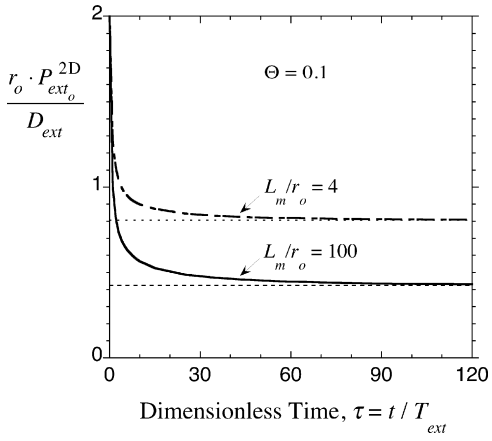

Fig. 4. Transient approach to steady-state for the external medium permeability predicted by the isolated medium 2D model. Displayed are the results of illustrative simulations for the clearance modulus value, $\Theta = 0.1$, representative of sucrose in the brain, and two values of the membrane aspect ratio spanning the approximate range for commercial microdialysis probes, $L_m/r_o = 4$ and 100. The dotted horizontal lines indicate the respective steady-state values of the permeability normalized using the effective diffusion coefficient in the tissue, D_{ext}. Time, t, is scaled relative to the diffusion time constant, $T_{ext} = r_o^2 \cdot K_{ext}/D_{ext}$, which for sucrose microdialysis in the brain is estimated to be 1.05 min (Table 4). The values for $L_m/r_o = 100$ are less than 5% above the values predicted for $L_m/r_o \to \infty$ from the radial diffusion model Eq. (20).

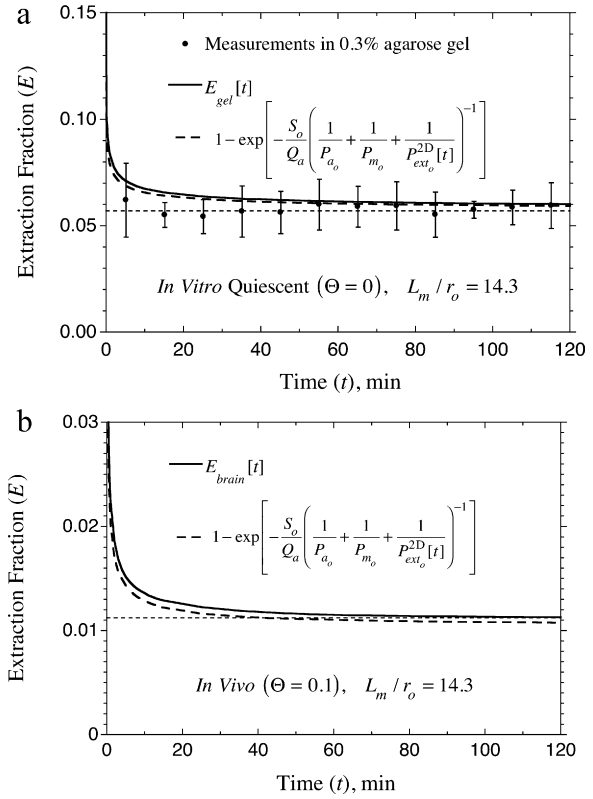

Fig. 5. Validation results for use of the transient external medium permeability to predict the time course in extraction fraction, E. (a) *In vitro*: sucrose microdialysis for probe in inert quiescent medium based on parameter values in Table 3. Solid circles are measurements for sampling from 0.3% agarose gel (mean ± SD, $n = 5$). (b) *In vivo*: sucrose microdialysis for probe in mouse brain based on parameter values in Table 4. The predictions from the full finite element model of Section 2.4 combining probe and external medium are given by the solid curves (transient) and horizontal dotted lines (steady-state). The dashed curves were obtained using the exponential expression for extraction fraction, Eq. (7) with the explicit steady-state permeability expressions for the annulus (P_{a_o}), Eq. (8), and the membrane (P_{m_o}), Eq. (10), and the transient isolated external medium 2D permeability values (P^{2D}_{exto}) from the finite element simulations of Section 2.3. The same probe with a length-to-radius ratio of $L_m/r_o = 14.3$ was modeled in both cases. The clearance modulus is denoted by Θ.

conditions. The *in vitro* results are displayed in Fig. 5(a) and *in vivo* values in Fig. 5(b). For both situations, finite element simulations were obtained for the full model 2D model of Section 2.4 and the isolated external medium 2D model of Section 2.3. The full model simultaneously simulates transport in the perfused probe and the external medium to predict the outflow concentration, c_{out}, given the inflow and external medium concentrations, c_{in} and c_{e_∞}. The isolated external medium model predicts the transient external medium permeability, which is then used together with the steady-state annulus and probe permeabilities to approximate the time course of the extraction fraction from Eq. (7). The good agreement between the two methods for calculating extraction fraction gives support for the validity of the isolated external medium approach. The decay in the extraction fraction is dominated by the external medium permeability transient as seen by the similarity in the shape of the curves between Figs. 4 and 5.

Superimposed in Fig. 5(a) are the extraction fraction values measured using probes inserted in 0.3% agarose gel in the experiments of Section 3.2. The measured values are in good agreement with the finite element predictions.

The contribution of each medium to the extraction fraction transient is related to the rate of change in the amount of sucrose in the media. Except at very early times, most of the change occurs in the external medium. In the *in vitro* case, the sucrose extracted by the probe is all coming from the amount initially present in the external medium. The rate of approach to the quasi-steady-state in Fig. 5(a) becomes very slow as the sucrose has to diffuse from greater distances. The *in vivo* case represents sucrose being supplied by uptake by the brain from the blood. At steady state no supply is occurring far from the probe because the distant tissue is in equilibrium with the blood. The sucrose arriving at the probe *in vivo* is coming from a much smaller volume of tissue than the volume of gel in the *in vitro* case.

The steady-state gel 2D permeability (0.012 cm/min) given in Table 3 is close to that of probe (0.014 cm/min), so both contribute about equally to determining the steady-state *in vitro* extraction fraction. However, the steady-state brain 2D permeability (0.0013 cm/min) is an order of magnitude smaller than the probe value. Consequently, the *in vivo* extraction fraction is dominated by the brain permeability. The difference in the relative magnitudes of the gel and brain permeabilities is the reason that the *in vitro* and *in vivo* extraction fractions in Fig. 5 differ by about a factor of five.

4.4. Spatial concentration profiles

Illustrative concentration profiles for the *in vitro* and *in vivo* cases are displayed in Fig. 6. The concentration profiles decay to essentially background levels within finite distances as a result of including axial diffusion in the 2D simulations. For the *in vivo* case with $\Theta = 0.1$, the penetration depth parameter, Γ, from Eq. (24) provides a useful measure of the extent of sucrose penetration into the surrounding tissue. The value is $\Gamma = 0.14$ cm and at this radial distance the midplane extracellular concentration at steady-state is about 90% of the uniform distant concentration. By contrast, the penetration depth parameter is of little utility for the *in vitro* case of the inert gel ($\Theta = 0$), since it has an infinite value ($\Gamma = \infty$). These findings underscore the importance of including axial diffusion in the modeling.

The relative magnitudes of the permeability values are reflected in the concentration drops across the respective media. For example, in the quiescent gel case about half of the concentration drop occurs across the probe and half across the gel, because the probe permeability from Table 2 is comparable in size to the quasi-steady-state gel permeability from Table 3. In the *in vivo* case, the

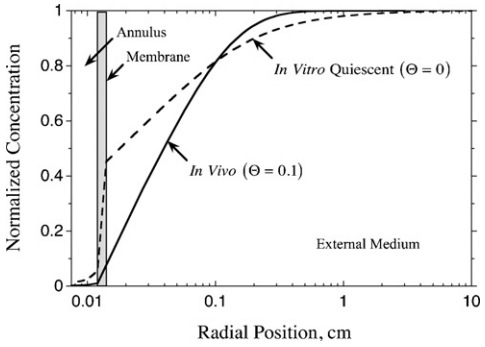

Fig. 6. Sucrose concentration profiles for sampling *in vivo* (brain) and *in vitro* (gel) from the 2D simulations of Fig. 5(a) and (b) for a probe of aspect ratio, $L_m/r_o = 14.3$. The steady-state concentration within the probe and the external medium is plotted versus the logarithm of radial distance from the probe axis at the midplane of the probe ($z = 0.1$ cm).

steady-state brain permeability from Table 4 is so much smaller than the probe permeability that almost all of the concentration drop occurs within the brain.

5. Conclusions

Including the axial contribution of analyte diffusion in the external medium is key to providing a comprehensive quantitative description of microdialysis jointly applicable to various *in vitro* and in *vivo* conditions. As illustrated in the present work, this can be accomplished for transient behavior through finite element analysis. One demonstration of the utility of finite element approaches combined modeling of both the probe and external medium. The simpler alternative simulated just the external medium in isolation. This latter approach generated transient permeability profiles for the external medium, which were then used together with steady-state probe permeability descriptions to predict the transient extraction fraction. The isolated external medium approach produced an algebraic expression that provides empirical estimates of the steady-state external medium permeability. This permits steady-state analyses to be performed without the need for additional finite element simulations. Among the additional advantages is an improved ability to compare results for probes with different membranes and different aspect ratios.

Acknowledgements

This research was supported [in part] by the Intramural Research Programs of the NIH, including the National Institute of Biomedical Imaging and Bioengineering. The authors are grateful to Paul F. Morrison for his critical review of the manuscript and suggestions for revision.

Appendix A. Equivalent sphere model for microdialysis

An earlier proposal to compensate for the deficiency in the radial diffusion model of Section 2.1 was to approximate the effect of 2D diffusion by replacing the accessible cylindrical outer surface of the membrane with a spherical surface of the same area [3]. The radius of this equivalent sphere is given by

$$\varpi_o = \sqrt{\frac{r_o \cdot L_m}{2}}. \tag{A.1}$$

The earlier analysis only considered the steady-state situation in which no mechanisms were present for eliminating analyte from the medium. Here the analysis is extended by including first order clearance processes and predicting transient behavior as well.

Reformulating the external medium mass balance Eq. (31) in spherical coordinates gives

$$\frac{\partial C[\varpi,\tau]}{\partial \tau} = \frac{1}{\varpi^2}\frac{\partial}{\partial \varpi}\left(\varpi^2 \frac{\partial C[\varpi,\tau]}{\partial \varpi}\right) - \Theta_s{}^2 C[\varpi,\tau], \tag{A.2}$$

in which the dimensional spherical radial coordinate, ϖ', is nondimensionalized as

$$\varpi \equiv \frac{\varpi'}{\varpi_o}, \tag{A.3}$$

the concentration is normalized as in Eq. (27)

$$C[\varpi,\tau] = \frac{c_e[\varpi,\tau] - c_{e_\infty}}{c_e[1,\tau] - c_{e_\infty}}, \tag{A.4}$$

and the modified clearance modulus is defined as

$$\Theta_s \equiv \varpi_o \sqrt{\frac{k_{ext}}{D_{ext}}}. \tag{A.5}$$

With the aid of Eq. (14.46) from Crank [14] the solution to Eq. (A.2) for the transient concentration profile is

$$C[\varpi,\tau] = \frac{\exp[-\Theta_s\cdot(\varpi-1)]\cdot \operatorname{erfc}\left[(\varpi-1/2\sqrt{\tau}) - \Theta_s\sqrt{\tau}\right]}{2\varpi} + \frac{\exp[\Theta_s\cdot(\varpi-1)]\cdot \operatorname{erfc}\left[(\varpi-1/2\sqrt{\tau}) + \Theta_s\sqrt{\tau}\right]}{2\varpi}. \tag{A.6}$$

Letting $\tau \to \infty$ in Eq. (A.6) and employing the limits $\operatorname{erfc}[\infty] = 0$ and $\operatorname{erfc}[-\infty] = 2$ yields the steady-state profile

$$C[\varpi,\infty] = \frac{\exp\left[-\Theta_s\cdot(\varpi-1)\right]}{\varpi}. \tag{A.7}$$

As in Eq. (19) the external medium permeability is defined by

$$\frac{\varpi_o \cdot P^{Sph}_{ext_o}}{D_{ext}} \equiv -\left(\frac{\partial C}{\partial \varpi}\right)_{\varpi=1}. \tag{A.8}$$

Substituting Eq. (A.6) into Eq. (A.8) leads to

$$\frac{\varpi_o \cdot P^{Sph}_{ext_o}[\tau]}{D_{ext}} = 1 + \Theta_s\cdot(1 - \operatorname{erfc}[\Theta_s\cdot\sqrt{\tau}]) + \frac{1}{\sqrt{\pi\tau}}\exp[-\Theta_s{}^2\cdot\tau]. \tag{A.9}$$

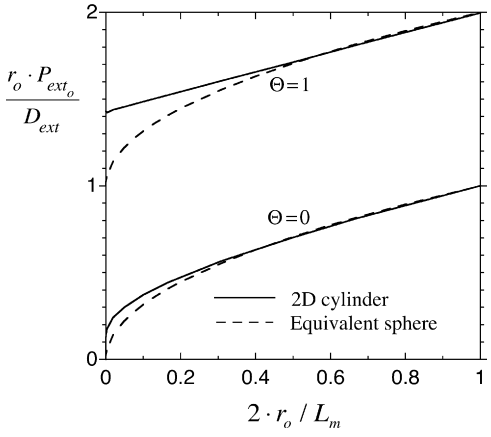

Fig. A1. Comparison of normalized external medium permeability predictions from the models that represent the probe membrane as a cylinder or a sphere of equivalent area. The normalized permeabilities are plotted against the inverse of the aspect ratio, L_m/r_o, for two illustrative values of the clearance modulus, Θ.

The predictions from the above equivalent sphere expressions can be related to those from 2D cylindrical coordinate analysis of Section 2.3 through the geometric interrelationships, Eq. (A.1), and

$$\Theta_s = \left(\frac{\varpi_o}{r_o}\right) \cdot \Theta = \sqrt{\frac{L_m}{(2 \cdot r_o)}} \cdot \Theta. \tag{A.10}$$

Substituting Eqs. (A.1) and (A.10) into Eq. (A.9) gives

$$\frac{r_o \cdot P_{ext_o}^{Sph}[\tau]}{D_{ext}} = \sqrt{\frac{2 \cdot r_o}{L_m}} \cdot \left\{ 1 + \sqrt{\frac{L_m}{2 \cdot r_o}}\Theta \cdot \left(1 - \mathrm{erfc}\left[\sqrt{\frac{L_m}{2 \cdot r_o}}\Theta \cdot \sqrt{\tau} \right] \right) + \frac{1}{\sqrt{\pi\tau}} \exp\left[-\frac{L_m}{2 \cdot r_o}\Theta^2 \cdot \tau \right] \right\}. \tag{A.11}$$

For steady state this simplifies to

$$\frac{r_o \cdot P_{ext_o}^{Sph}}{D_{ext}} = \sqrt{\frac{2 \cdot r_o}{L_m}} + \Theta. \tag{A.12}$$

As illustrated in Fig. A1 the predictions from Eq. (A.12) are in good agreement with those from the 2D simulations for short probes ($2 \cdot r_o/L_m \sim 1$), but diverge for long probes ($2 \cdot r_o/L_m \to 0$). The agreement is better over more of the aspect ratio range for inert quiescent conditions, $\Theta = 0$, for which the equivalent sphere model was originally proposed.

References

[1] G. Amberg, N. Lindefors, J. Pharmacol. Methods 22 (1989) 157–183.
[2] H. Benveniste, A.J. Hansen, N.S. Ottosen, J. Neurochem. 52 (1989) 1741–1750.
[3] P.M. Bungay, P.F. Morrison, R.L. Dedrick, Life Sci. 46 (1990) 105–119.
[4] P.F. Morrison, P.M. Bungay, J.K. Hsiao, B.A. Ball, I.N. Mefford, R.L. Dedrick, J. Neurochem. 57 (1991) 103–119.
[5] P.F. Morrison, P.M. Bungay, J.K. Hsiao, I.N. Mefford, K.H. Dykstra, R.L. Dedrick, in: T.E. Robinson, J.B. Justice Jr. (Eds.), Microdialysis in the Neurosciences, Elsevier, New York, 1991, pp. 47–80.
[6] F. Wallgren, G. Amberg, R.C. Hickner, U. Ekelund, L. Jorfeldt, J. Henriksson, J. Appl. Physiol. 79 (1995) 648–659.
[7] K.C. Chen, M. Höistad, J. Kehr, K. Fuxe, C. Nicholson, J. Neurochem. 81 (2002) 94–107.
[8] K.C. Chen, M. Höistad, J. Kehr, K. Fuxe, C. Nicholson, J. Neurochem. 81 (2002) 108–121.
[9] P.M. Bungay, P.F. Morrison, R.L. Dedrick, V.I. Chefer, A. Zapata, in: B.H.C. Westerink, T.I.F.H. Cremers (Eds.), Handbook of Microdialysis: Methods, Applications and Perspectives, Academic Press/Elsevier, Amsterdam, 2007, pp. 131–167.
[10] S. Tong, F. Yuan, J. Pharm. Biomed. Anal. 28 (2002) 269–278.
[11] P.M. Bungay, R.A. Gonzales, in: 26th Annual Meeting of the Society for Neuroscience, Washington, DC, 1996, p. 2076.
[12] P.M. Bungay, T. Wang, H. Yang, W.F. Elmquist, J. Membr. Sci. 348 (2010) 131–149.
[13] M. Abramowitz, I.A. Stegun, Handbook of Mathematical Functions, Applied Mathematics Series, vol. 55, National Bureau of Standards (U.S. Government Printing Office), Washington, DC, 1964, pp. 355–433.
[14] J. Crank, The Mathematics of Diffusion, second ed., Oxford Science Publications, New York, 1975, p. 334.
[15] C. Nicholson, Rep. Prog. Phys. 64 (2001) 815–884.
[16] M. Höistad, K.C. Chen, C. Nicholson, K. Fuxe, J. Kehr, J. Neurochem. 81 (2002) 80–93.